ACS Catalysis

Research Article

pubs.acs.org/acscatalysis

Mechanistic Studies of ε-Caprolactone Polymerization by (salen)AlOR Complexes and a Predictive Model for Cyclic Ester Polymerizations

Elodie E. Marlier, Joahanna A. Macaranas, Daniel J. Marell, Christine R. Dunbar, Michelle A. Johnson, Yvonne DePorre, Maria O. Miranda, Benjamin D. Neisen, Christopher J. Cramer,* Marc A. Hillmyer,* and William B. Tolman*

Department of Chemistry, Center for Sustainable Polymers, Chemical Theory Center, and Minnesota Supercomputing Institute, University of Minnesota, 207 Pleasant Street SE, Minneapolis, Minnesota 55455, United States

Supporting Information

ABSTRACT: Aluminum alkoxide complexes (**2**) of salen ligands with a three-carbon linker and para substituents having variable electron-withdrawing capabilities (X = NO_2, Br, OMe) were prepared, and the kinetics of their ring-opening polymerization (ROP) of ε-caprolactone (CL) were investigated as a function of temperature, with the aim of drawing comparisons to similar systems with two-carbon linkers investigated previously (**1**). While **1** and **2** exhibit saturation kinetics and similar dependences of their ROP rates on substituents X (invariant K_{eq}, similar Hammett ρ = +1.4(1) and 1.2(1) for k_2, respectively), ROP by **2** was significantly faster than for **1**. Theoretical calculations confirm that, while the reactant structures differ, the transition state geometries are quite similar, and by analyzing the energetics of the involved distortions accompanying the structural changes, a significant contribution to the basis for the rate differences was identified. Using this knowledge, a simplified computational method for evaluating ligand structural influences on cyclic ester ROP rates is proposed that may have utility for future catalyst design.

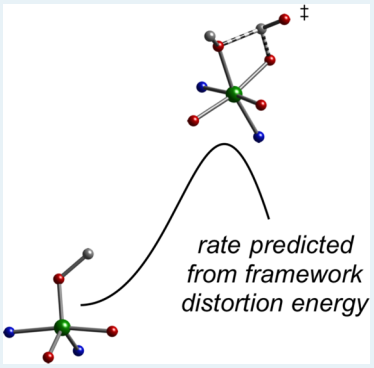

KEYWORDS: *ring-opening polymerization, catalysis, ligand effects, computation, saturation kinetics*

INTRODUCTION

Through the controlled ring-opening polymerization of cyclic esters, a variety of useful and often renewable polymers may be synthesized.[1,2] Among the catalysts found to be effective in such polymerization reactions, metal alkoxides are ubiquitous and in many cases operate at high rates with excellent control of polymer molecular weight and stereochemistry.[2b−h] Further improvements in catalytic behavior by metal alkoxide catalysts are likely if the mechanism(s) of ROP is (are) understood and the roles of supporting ligand structural variation on ROP rates and selectivities are unraveled. Toward that end, numerous mechanistic studies have been reported, leading to the hypothesis of the often used and generic "coordination−insertion" pathway (Scheme 1), wherein binding of the ester to the metal (coordination) is followed by nucleophilic attack and ring opening (insertion).[2,3] However, the involvement of these two sequential independent steps has been difficult to confirm and evaluation of the influences of ligand variation on them has been impeded because comparisons are typically made on the basis of measured pseudo-first-order rate constants (k_{app}) that are composites of equilibrium and/or rate constants for the attendant elementary reaction steps. Nonetheless, intriguing effects of changes in ligand structure on ROP k_{app} values have been seen. A notable example is a study of *rac*-lactide (LA) polymerization using aluminum alkoxide catalysts derived from treatment of (salen)AlMe complexes with benzyl alcohol (Figure 1, top);[4] such aluminum alkoxide catalysts are known to be mononuclear, single-site species that operate at rates convenient for measurement by routine NMR methods. Rates of LA ROP increased when $R_1 = R_2$ = Cl versus H or *t*-Bu (with identical linkers X), consistent with the enhanced electrophilicity of the metal center underlying higher k_{app} values. The rates also increased as the linker was changed from two to three carbons (X = $-CH_2C(Me)_2-$ vs $-CH_2C(Me)_2CH_2-$), but on the basis of the data available the only conclusion drawn was that "the enhanced performance of the C_3 linker is more a function of the flexibility of the linking unit, which may allow the complex to better access the key transition states involved in the ROP process".[4]

Scheme 1. Generalized Coordination−Insertion Mechanism

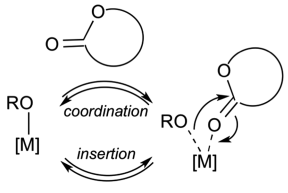

Received: November 18, 2015
Revised: January 6, 2016
Published: January 21, 2016

DOI: 10.1021/acscatal.5b02607
ACS Catal. 2016, 6, 1215−1224

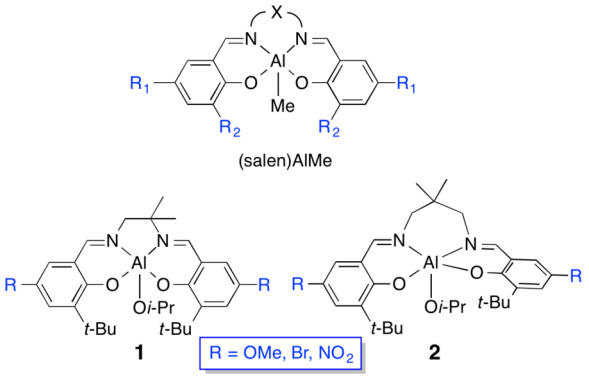

Figure 1. Generalized structures of (salen)AlMe complexes studied as LA polymerization precursors (top)[4] and catalysts **1** and **2** used in mechanistic studies of CL polymerization (bottom).

We have sought more detailed mechanistic information for such cyclic ester polymerizations by mononuclear aluminum alkoxide complexes through dissection of composite k_{app} values into kinetic/thermodynamic constants associated with elementary reaction steps.[5,6] Through such studies, we aim to better understand the fundamental basis for ROP rate differences caused by catalyst structure variation in compounds that are single-site catalysts, with the ultimate goal of applying this knowledge to the design of more effective catalysts. In previous work,[6] we examined the kinetics of ε-caprolactone (CL) polymerization by mononuclear aluminum alkoxide complexes **1** (Figure 1) using high monomer concentrations ($[CL]_0 \geq 2.0$ M). Under these conditions, saturation behavior was observed, and the data could be fit to the rate law eq 1 (PCL = polycaprolactone) to provide values of the equilibrium constant for monomer binding, K_{eq}, and the rate constant for monomer enchainment, k_2, as a function of temperature and remote substituent R. While K_{eq} varied little as a function of the electron-withdrawing properties of R (Hammett $\rho = +0.16(8)$), the k_2 dependence was significantly larger ($\rho = +1.4(1)$), supporting the hypothesis that differences in k_2 underly observed overall rate differences and that k_2 is enhanced by increased electrophilicity of the metal center. Density functional theory (DFT) revealed transition state (TS) structures featuring bond formation between the alkoxide and the incoming carbonyl of CL, showing that greater electron withdrawal by the substituent on the salen ligand results in greater bonding between the nucleophilic alkoxide and the lactone carbonyl carbon in the TS to give enhanced polymerization rates, and indicated that K_{eq} was not appropriately assigned to formation of a CL adduct along the reaction pathway; instead, K_{eq} is associated with "non-productive" binding that inhibits the ROP rate at high substrate concentrations.

$$-\frac{d[CL]}{dt} = \frac{d[PCL]}{dt} = \frac{k_2[\mathbf{2}][CL]}{1/K_{eq} + [CL]} \quad (1)$$

To dissect the intriguing effect of linker length described in the previous studies,[4] we have now applied our saturation kinetics approach to ROP by **2**, comprising the same substituents as **1** but with a longer ligand linker. As described below, we observed saturation kinetics for CL polymerization by **2** that were fit to eq 1 to yield K_{eq} and k_2 values as a function of temperature. Comparison of these values to those reported previously for **1**,[6] in concert with evaluation of reactant and transition-state structures via DFT, provided additional detailed insight into how linker length affects ROP, with intriguing implications for future ROP catalyst design.

RESULTS

Synthesis and Characterization of Ligands and Complexes. The proligands H_2L^R (R = OMe, Br, NO_2) and their complexes **2** were prepared according to the same procedures described previously for **1**,[6] except using 2,2-dimethyl-1,3-propanediamine in the condensations with the respective salicylaldehydes. The proligands were isolated as bright yellow crystalline solids in good yields (70–91%) and then heated with Al(O-*i*-Pr)$_3$ in toluene to afford the compounds **2**, which were isolated as analytically pure bright yellow, yellow, and light brown solids (R_1 = OMe, Br, NO_2, respectively), also in good yields (72–90%). The proligands and complexes were characterized by ^{1}H, {^{1}H}^{13}C, and ^{27}Al NMR spectroscopy, CHN analysis, and, for **2** (R = Br), X-ray crystallography. The X-ray structure (Figure 2) confirms the anticipated five-coordinate formulation with a τ value of 0.84,[7] close to idealized trigonal bipyramidal (τ =1) and similar to that of related complexes of salen ligands also featuring the 2,2-dimethylpropyl linker.[4,8] The τ value differs from that previously determined for **1** (R = OMe; τ = 0.52)[6] and other closely related congeners with a two-carbon linker (τ = 0.48–0.56).[4,8a,b] Density functional theory optimization of **2** (R = H; see Density Functional Calculations for theoretical details) provided a τ value of 0.85, which is in excellent agreement with that determined from crystallography, suggesting that crystal packing forces do not significantly influence the intrinsic coordination geometry at the aluminum center.

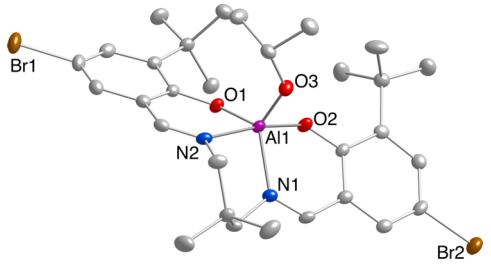

Figure 2. Representation of the X-ray crystal structure of **2** (R = Br), showing all non-hydrogen atoms as 50% thermal ellipsoids. Selected interatomic distances (Å) and angles (deg): Al1–O1, 1.7803(17); Al1–O2, 1.8225(18); Al1–O3, 1.7345(19); Al1–N1, 2.054(2); Al1–N2, 1.994(2); O3–Al1–O2, 95.76(9); O3–Al1–O1, 120.96(9); O2–Al1–O1, 91.22(8); O3–Al1–N1, 92.35(9); O2–Al1–N1, 171.10(9); O1–Al1–N1, 87.74(8); O3–Al1–N2, 118.71(9); O2–Al1–N2, 88.90(8); O1–Al1–N2, 119.98(9); N1–Al1–N2, 83.98(8).

The ^{1}H NMR spectra for the complexes **2** (Figures S1–S6 in the Supporting Information) are consistent with monomeric structures and contain a single resonance for the *tert*-butyl groups, indicating that the two different chemical environments of the aryl groups in the experimentally determined X-ray structure for **2** (R = Br) and calculated gas-phase structures for **2** (R = H) are averaged in solution. Such fluxionality was reported for other complexes of related salen ligands with the 2,2-dimethylpropyl linker.[4,8] The NMR spectra of the complexes **2** with different R groups are generally similar, except for differences in the aryl region (imine hydrogens and two aromatic hydrogens adjacent to R). The ^{27}Al NMR spectra

DOI: 10.1021/acscatal.5b02607
ACS Catal. 2016, 6, 1215–1224

contain a single resonance at 35, 34, and 33 ppm for the complexes with R = OMe, Br, NO_2, respectively.

Kinetics of CL Polymerizations. NMR-scale polymerization reactions for each catalyst were run in triplicate at four different temperatures ranging from 273 to 313 K. The reactions were performed in toluene-d_8 with a fixed initial concentration of monomer ([CL] = 2.0 M), catalyst ([cat] = 5.5−7.0 mM), and internal standard ([1,4-bis(trimethylsilyl)-benzene] = 4.0 mM), with growth of polymer (PCL) and decay of monomer (CL) monitored throughout the reaction by ^{1}H NMR spectroscopy. Most polymerizations achieved 99% conversion, except for those catalyzed by **2** (R = NO_2) at 273 K, for which the loss of NMR shims only allowed for analysis up to only about 84% conversion. Similarly to previous work,[5,6] the concentrations of CL and PCL (determined by integrations vs the standard) were plotted versus time and fit to eq 1 using the global kinetics fitting program COPASI (Figures S7−S11 in the Supporting Information). A reaction progress kinetic analysis (RPKA)[9] protocol was used to analyze one polymerization run (R = Br, 273 K) and further supported the appropriateness of eq 1 (Figure S12 and Table S2 in the Supporting Information), with fits to alternative first- and second-order rate laws being notably inferior (Figure S13 in the Supporting Information). Average values from the triplicate runs for the kinetic parameters K_{eq} and k_2 calculated from the COPASI fits to eq 1 are compiled in Table 1; the complete list of parameters from both COPASI analysis and RPKA are provided in Table S1 in the Supporting Information.

Table 1. Average Values for Kinetic Parameters K_{eq} and k_2 for Complexes 2

			K_{eq} (M^{-1})		
entry	temp (K)	R	COPASI	NMR	k_2 (s^{-1})
1	313	OMe	3.4(7)	0.65(9)	0.32(2)
2	298	OMe	3.8(7)	0.64(5)	0.147(5)
3	293	OMe	3.3(4)	0.69(4)	0.105(3)
4	283	OMe	4.0(5)	0.88(3)	0.048(3)
5	298	Br	1.4(3)	0.6(1)	0.67(6)
6	293	Br	1.3(2)	1.2(4)	0.53(4)
7	283	Br	1.5(2)	0.9(2)	0.27(2)
8	273	Br	1.7(2)	0.65(8)	0.106(6)
9	293	NO_2	0.8(4)	1.9(5)	1.9(7)
10	288	NO_2	0.5(2)	1.6(3)	1.9(6)
11	278	NO_2	0.9(3)	1.9(2)	0.6(2)
12	273	NO_2	0.7(5)	1.7(5)	0.5(2)

The presence of a substrate binding equilibrium characterized by K_{eq} was further confirmed by two independent sets of experiments. First, we analyzed the chemical shifts of peaks associated with the catalyst during the polymerization reaction. Changes in the chemical shifts of the catalyst peaks as a function of [CL] were observed, and we analyzed them as described previously,[5,6] working under the assumption that these changes arise from rapid equilibration between complexes with and without bound monomer. Typical ^{1}H NMR spectra and plots of chemical shift vs [CL] are presented in Figures S14−S17 in the Supporting Information, and calculated average K_{eq} values are given in Table 1 (a full list is given in Table S3 in the Supporting Information). Although the K_{eq} values independently determined from the catalyst NMR peak analysis and those obtained from the kinetic fits (COPASI) of the CL decay and PCL generation profiles to eq 1 are not identical, we consider them to be sufficiently similar to be consistent with the hypothesized substrate binding equilibration, especially if one considers the narrow span of derived ΔG° values (see below).

In a second set of experiments, complexes **2** were mixed at 293 K with varying concentrations of γ-butyrolactone (BL), a cyclic ester that is relatively unreactive toward ring-opening polymerization.[10] The chemical shifts of the ligand peaks in the aromatic region were observed to change as a function of [BL], consistent with a binding equilibrium. Fitting of the data accordingly yielded K_{eq} values of 0.6(1), 0.5(2), and 0.9(2) for R = OMe, Br, NO_2, respectively (Figures S18 and S19 in the Supporting Information). The relatively good agreement among the K_{eq} values determined from fitting of the kinetic profiles and analysis of the catalyst NMR peaks during CL polymerization and in the presence of BL provides strong experimental evidence for equilibrium binding of lactones to the catalysts **2** (Table S4 in the Supporting Information).

Evaluation of the variation of the experimentally determined kinetic and thermodynamic parameters as a function of substituent R and temperature provided important insights. A plot of ln K_{eq} versus $1/T$ including values from both COPASI (circles) and NMR analysis (squares) shows clustering of ln K_{eq} values within a relatively narrow range (−0.5 to +1.5) and with minimal temperature dependences indicative of relatively small ΔG° values of <2 kcal mol^{-1} for monomer binding (Figure 3).

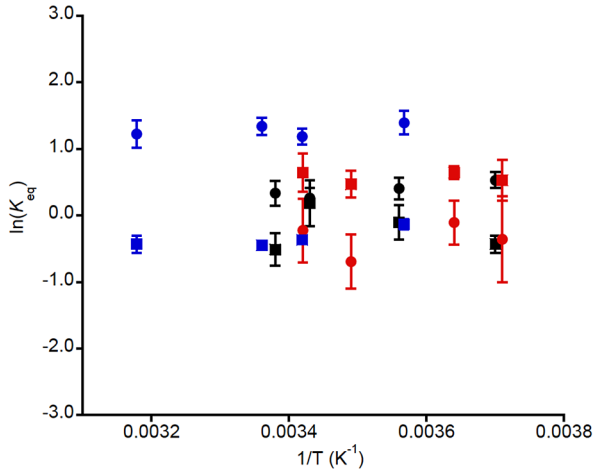

Figure 3. Plot of ln K_{eq} versus $1/T$ for **2** (R = Br, black; R = OMe, blue; R = NO_2, red), using K_{eq} values determined via kinetic fits (COPASI, circles) and via fits of catalyst peak chemical shifts in NMR spectra (NMR, squares).

The K_{eq} values determined by COPASI as a function of R are ordered OMe > Br > NO_2, but the differences are small and this ordering is not followed using the values determined by the NMR method. Thus, as reported previously for **1**,[6] we conclude that the thermodynamics for binding of CL to **2** are relatively insensitive to substituent R, consistent with differences in CL binding not being an important basis for the differences in the observed polymerization rates.

The temperature dependences of the rate constants k_2 for the polymerizations of CL by **2** (this work, circles) and **1** (squares)[6] are shown in Figure 4, and activation parameters determined from linear fits to the Eyring equation are given in Table 2. It is readily apparent from the Eyring plots in Figure 4 and the derived $\Delta G^{\ddagger}_{298}$ values that the polymerization rate

DOI: 10.1021/acscatal.5b02607
ACS Catal. 2016, 6, 1215−1224

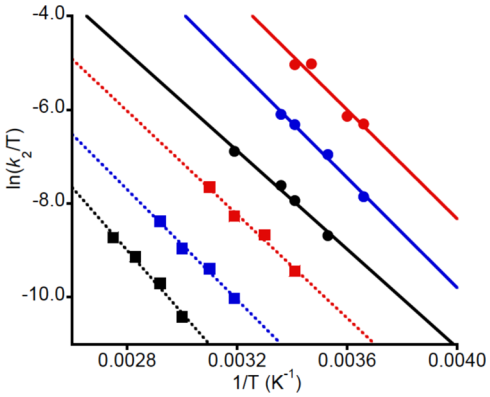

Figure 4. Eyring plots of $\ln(k_2/T)$ versus $1/T$ for **1** (squares, dashed lines) and **2** (circles, solid lines) for R = OMe (black), Br (blue), and NO_2 (red).

Table 2. Activation Parameters (k_2) for the Polymerization of CL

catalyst	R	$\Delta H^{\ddagger a}$	$\Delta S^{\ddagger b}$	$\Delta G^{\ddagger a}$ (298 K)
2[c]	OMe	9.1 ± 0.3	−32 ± 1	18.6 ± 0.4
2[c]	Br	10.4 ± 0.4	−24 ± 1	17.6 ± 0.5
2[c]	NO_2	10.0 ± 0.9	−23 ± 3	17 ± 1
1[d]	OMe	13.5 ± 0.5	−27 ± 2	21.5 ± 0.8
1[d]	Br	11.5 ± 0.3	−30 ± 2	20.4 ± 0.7
1[d]	NO_2	10.8 ± 0.4	−27 ± 2	18.8 ± 0.7

[a]In kcal mol^{-1}. [b]In cal mol^{-1} K^{-1}. [c]Determined from the linear fits in Figure 4 using the Eyring equation. [d]Reference 6.

constants are greater for **2** than for **1**. From the activation parameters, we calculate that the fastest catalyst **2** (R = NO_2) and the slowest catalyst **1** (R = OMe) have k_2 values that differ by factors of ~(1−5) × 10^3 (350−273 K). Hammett plots of log k_2 versus σ_p for **2** are linear at all temperatures with similar positive slopes (Figure 5), yielding an average ρ value of

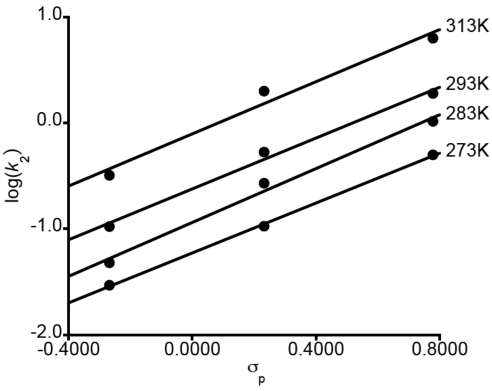

Figure 5. Hammett plots of $\log(k_2)$ versus σ_p for the polymerization of CL by **2** at the indicated temperatures.

+1.2(1) that is similar to that reported previously for **1** (+1.4(1)).[6] Thus, the sensitivities of the rate constants to the electronic influences of the ligand substituents R are similar for the two catalyst systems.

Theoretical Modeling. To gain additional insight into the observed catalytic activities, and in particular to better understand the rate accelerations observed relative to the first-generation catalyst **1**, we undertook density functional characterization of reaction pathways associated with catalyst **2** (see the Experimental Section for full computational details). For computational simplicity, we modeled the alkoxide in the precatalyst as MeO instead of *i*PrO, and to differentiate this we refer to the MeO-substituted precatalyst structures as **1′** and **2′** below.

Conformational Flexibility of Catalyst. In comparison to **1′** with its two-carbon backbone linker, a number of alternative chair and twist-boat conformations of the three-carbon backbone are available to the ligand in **2′**. In particular, for the precatalyst carrying no para substituents on the aromatic rings, we identified four different conformations (three twist-boats and one chair), spanning a range in electronic energy of 2.2 kcal/mol. Both the lowest and highest energy conformations were found to be twist boats (the lowest is shown in Figure 6), with the chair conformation being intermediate in

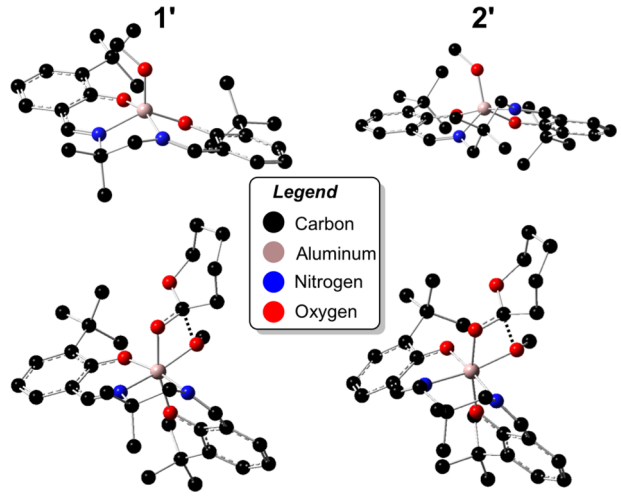

Figure 6. DFT predicted lowest-energy structures for *p*-H-substituted **1′** and **2′** (above) and for their corresponding transition-state structures for ring opening of CL (below). H atoms are omitted for clarity.

energy. A Boltzmann average over all four conformers leads to a reduction in the free energy of the population of free catalyst structures of only 0.1 kcal/mol: i.e., the global minimum sits reasonably far below the other conformers in energy. We applied the same 0.1 kcal/mol correction to the energies of the global minimum twist boats in the para-substituted cases, assuming the influence of para substitution on the conformational energetics to be minimal.

Catalysis. To characterize the mechanism of ROP with the catalyst **2′**, we carried out an exhaustive search over all of the pathways associated with the various possible catalyst/CL stereochemical orientations analogous to a prior study involving catalyst **1′**.[6] We observed again that one particular orientation, which was referred to as "pathway 6" in our prior work,[6] led to CL ring opening through a transition-state (TS) structure having the lowest activation free energy of all those surveyed (Figure 6). Indeed, for the model system lacking para substituents, $\Delta G^{\ddagger}$ along pathway 6 was predicted to be at least 4 kcal/mol lower than any other pathway investigated, suggesting that Boltzmann averaging over alternative stereochemistries is not required for the modeling of the transition state. The TS structures in **1′** and **2′** are overall quite similar: in each case, there is roughly octahedral coordination about Al with an O−Al−O angle involving the alkoxide and carbonyl

DOI: 10.1021/acscatal.5b02607
ACS Catal. 2016, 6, 1215−1224

oxygen atoms of about 75° and with both Al−O bond lengths being 1.92 ± 0.01 Å. Full details of all bond lengths and angles are provided in Figure S20 in the Supporting Information, and additional analysis of the similarity of TS structure geometries across a wider range of Al-based catalysts is provided below in the Discussion.

Rate Acceleration in Catalyst 2′. Predicted free energies of activation for the reaction of catalyst **2′** with CL are provided in Table 3 for the cases of *p*-OMe, *p*-Br, and *p*-NO_2 substitution at

Table 3. Predicted 298 K Activation Free Energies (kcal/mol) for Reaction of 1′ and 2′ with CL

para substituent	1′	2′
MeO	12.4	9.7
Br	11.1	8.2
NO_2	9.6	5.9

298 K. Also included in Table 3 are the analogous predictions previously reported for catalyst **1′**. Experimentally, a rate acceleration of about 3 orders of magnitude is observed on going from **1** to **2** with identical para substituents, which corresponds to a lowering of the activation free energy by about 4 kcal/mol at 298 K. As can be seen in Table 3, we predict reductions in activation free energies of 2.7, 2.9, and 3.7 kcal/mol for the *p*-MeO-, *p*-Br-, and *p*-NO_2-substituted cases of **2′**, respectively. These reductions (in what is effectively K_{eq}*k_2, since we compute activation free energies relative to infinitely separated reactants) are in generally good agreement with experimental observations (cf. Table 2, noting that variations in k_2 have a larger influence on relative rates than K_{eq}; cf. Table 1), although the acceleration predicted for the *p*-NO_2-substituted system is somewhat larger. Focusing only on para substitution effects in **2** itself, experiment shows an acceleration relative to R = MeO of −1.1 and −1.5 kcal/mol for R = Br and R = NO_2, respectively. Theory predicts values of −1.5 and −3.8 kcal/mol for **2′**, again in reasonably good agreement with experiment, albeit with some overestimation of the rate acceleration afforded for the *p*-NO_2 case.

Saturation Kinetics. Experimental measurements indicate that there is a modest equilibrium constant for the complexation with CL of all three para-substituted derivatives of **2** examined here. This is similar to the situation previously described for **1**,[6] where DFT identified many local minimum structures corresponding to van der Waals complexes between CL and **1′**. In that case, the lowest energy such structure involved CL binding trans to the methoxide ligand, generating a structure that is necessarily incapable of ring opening; thus, the saturation kinetics observed were interpreted as substrate inhibition. In the case of **2′**, on the other hand, no such trans complexes with CL proved to be especially favorable—while van der Waals structures having CL on the side of **2** opposite MeO could be located, they were no lower in energy than alternative structures with CL on the same face as MeO, likely owing to steric constraints diminishing favorable interactions between Al and the carbonyl oxygen of CL (the shortest distance found between these two atoms for a trans complex was 2.26 Å; see Figure 7). However, saturation kinetics is predicted for reactions having a pre-equilibrium irrespective of whether that equilibrium leads to unreactive or reactive structures, and in this respect the kinetics of **2′** in comparison to those of **1′** are rationalized as deriving from a still-sizable population of prereactive complexes.

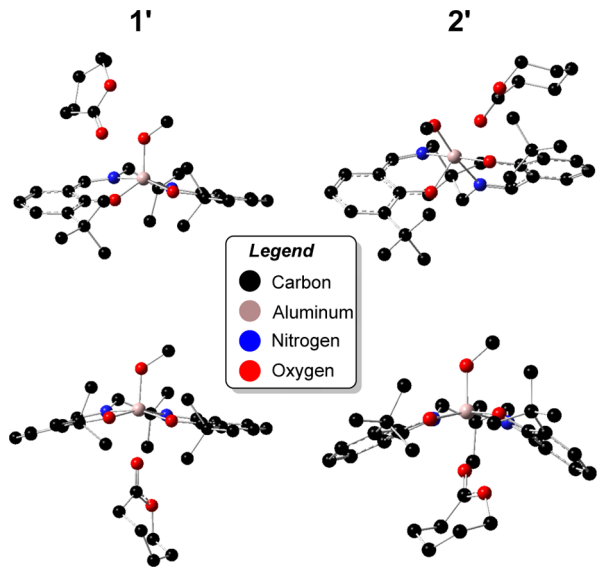

Figure 7. Representative M06-L same-face and opposite-face van der Waals complexes of CL with **1′** and **2′**. In the case of **1′**, the trans complex is lower in free energy than the same-face structure by 8.4 kcal/mol. In the case of **2′**, the trans complex is higher in free energy by 7.0 kcal/mol.

DISCUSSION

In delving into the detailed effects of the change in ligand linker from two carbons to three on the rate of CL polymerization by **1** and **2**, respectively, we used a combination of experimental and theoretical approaches to compare the structures of the reactants, their saturation kinetics behavior as a function of para substituent and temperature, and the nature of relevant ring-opening transition states. X-ray crystallography and theory confirmed that the longer linker in **2** results in a coordination geometry closer to trigonal bipyramidal (τ = 0.84) in comparison to **1** (τ = 0.52). This structural effect had been noted previously but discounted as a rationale for different LA polymerization rates because rate accelerations did not occur with (salen)AlMe precatalysts with similar τ values but with rigid rather than flexible linkers.[4] As seen for **1**, we observed saturation behavior in the kinetics of CL polymerization by **2**, and the combined evidence from kinetic fits and NMR data for **2** in the presence of γ-butyrolactone (BL), which does not polymerize under the conditions explored, supports assignment of K_{eq} to equilibrium monomer binding. For **1**, theory suggests that the lowest energy complex-binding monomer is unable to proceed to polymerization (owing to trans binding) and is thus inhibitory. For **2**, theory predicts that trans binding is *not* competitive with productive binding, and K_{eq} instead is a measure of alternative prereactive bound complexes. Nonetheless, the relevant kinetic behavior is the same in these two situations: i.e., saturation kinetics is predicted and observed. Importantly, we conclude that differences in CL polymerization rates between **1** and **2** and among systems with different para substituents R do not arise from differences in K_{eq} because these values do not vary significantly as a function of linker length (**1** vs **2**), R (OMe, Br, or NO_2), or temperature. Instead, the overall rate differences arise from variations in k_2. While the sensitivity of k_2 to the electron-withdrawing ability of substituent R is similar for systems **1** and **2** (Hammett ρ values of +1.4(1) and +1.2(1), respectively), and this supports similar mechanisms for CL polymerization by these two

DOI: 10.1021/acscatal.5b02607
ACS Catal. 2016, 6, 1215−1224

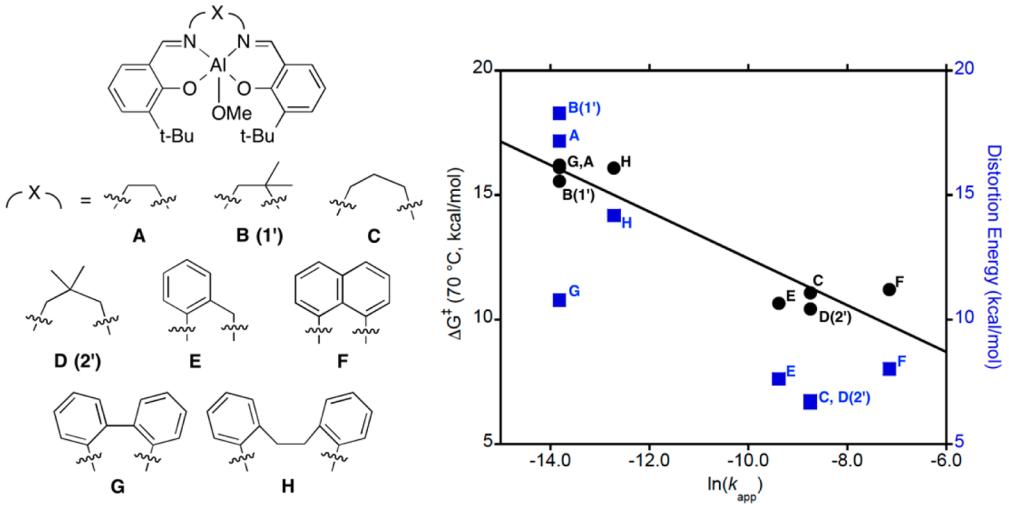

Figure 8. Relationship between ln k_{app} for a series of ROP catalysts described by Gibson et al.[4] (but lacking the *t*-Bu groups para to the phenolate donors) and computed activation free energies (black circles) and framework distortion energies (blue squares) for corresponding reactant and TS structures. The best-fit line to the activation free energies has the Pearson correlation coefficient R = 0.947. The best-fit line to the framework distortion energies (not shown) has R = 0.852.

systems, at parity of R the rates of CL polymerization by **2** are significantly faster.

To rationalize the rate acceleration observed with **2** in comparison to **1**, we focused more closely on the geometric details associated with the ring-opening TS structures in each instance.[11] As noted above and quantified in Figure S20 in the Supporting Information, for the two different TS structures the geometry about the catalytic Al center is predicted to be quite similar: the mean unsigned deviation over all Al−X bond lengths is 0.01 Å and the mean unsigned deviation over all (cis) X−Al−Y angles is 3.0°. This observation suggests that each catalyst is able to achieve a common geometry that is optimal for reducing the free energy of activation of ring opening. It also raises the question, then, of what is required in terms of distortion energy relative to the resting precatalyst structure to *arrive* at this optimal geometry. Also shown in Figure S20 are corresponding metrics for the resting precatalysts **1**′ and **2**′, and it is clear that there are more substantial geometric differences between these alkoxide complexes than there are between the corresponding TS structures. The differences are primarily associated with the degree of square-pyramidal vs trigonal-bipyramidal character imposed by the different ligands and are well captured by the different τ values reported above (experimental and calculated).

To address the question of the influence of required distortion from precatalyst to TS structure in more quantitative detail, for both **1**′ and **2**′ we removed the reacting partners and the MeO units from the optimized TS structures, and we carried out single-point calculations on the resulting cationic conformers of the catalyst frameworks to determine their differences in energy relative to the precatalyst from which the MeO unit had been removed. This calculation thereby provides an approximation to the distortion energy of the aluminum−ligand framework that is associated with adoption of a geometry well suited to stabilize the optimal TS structure. The framework of **1** requires 18.3 kcal/mol to distort from the precatalyst structure to the TS structure, while the framework of **2** has a corresponding distortion energy of only 6.8 kcal/mol. Clearly, then, the "resting" framework of **2** is much closer to the optimal catalytic geometry than is that of **1**. This computed difference is considerably larger than the experimentally observed rate acceleration, as might be expected insofar as differential alkoxide interactions with the catalyst resting geometries would be expected to act in some way to reduce differential strain. Nevertheless, the striking difference that is computed suggests that enhanced catalytic activity can be engineered through the design of catalysts whose precomplexed structures are already geometrically similar to the octahedral TS structures determined from DFT to have the lowest activation free energies for ring-opening polymerization.

To assess further the relative utility of this framework-strain analysis for the prediction of catalyst activity, we examined another six related ROP catalysts reported previously (structures in Figure 8).[4] In each instance, we computed precatalyst and TS structures analogous to those for **1**′ and **2**′. In all eight TS structures, there was a remarkable uniformity in the 12 unique cis valence bond angles about Al. For example, for the O−Al−O valence angle between the alkoxide and caprolactone carbonyl oxygen atoms, the average and standard deviation were found to be 74.8 ± 0.7° over all eight structures. The largest angular standard deviation, 4.7°, was associated with the N−Al−N valence angle, which is unsurprising given the variation in bridge lengths in the various catalysts; for all remaining angles, the standard deviations ranged from 0.6 to 2.3°.

This similarity in TS structures prompted us to explore further the utility of our distortion energy hypothesis. Thus, we removed the same alkoxide and CL components and computed distortion energies for the six additional compounds[4] analogous to those already described for **1**′ and **2**′ (Figure 8). These distortion energies, as well as the computed activation free energies, are plotted vs the natural logarithm of the previously reported[4] lactide ROP rate constants (for catalysts that contain *t*-Bu groups para to the phenolate donor) determined under equivalent conditions in Figure 8 (together with the calculated data for **1**′ and **2**′ already described above).

There is a good correlation between the computed activation free energies and the observed ln k_{app} values, providing further validation of the modeling protocol. Interestingly, the correlation of the rate constant data with the framework

DOI: 10.1021/acscatal.5b02607
ACS Catal. 2016, 6, 1215−1224

distortion energies is also fairly good. Indeed, *if* the data point for catalyst **G** is removed, the Pearson correlation coefficient for the latter correlation is predicted to be identical with that for the activation free energies (R = 0.947). For this outlier, a significantly lower distortion energy is predicted than for catalysts **A** and **B**, even though all three are found experimentally to catalyze ROP at essentially identical rates. This suggests that there is an interaction in the actual TS structure for **G** that destabilizes the structure beyond distortion of the framework. Indeed, if one examines a space-filling model of the TS structure for polymerization of CL by **G** (Figure 9) it

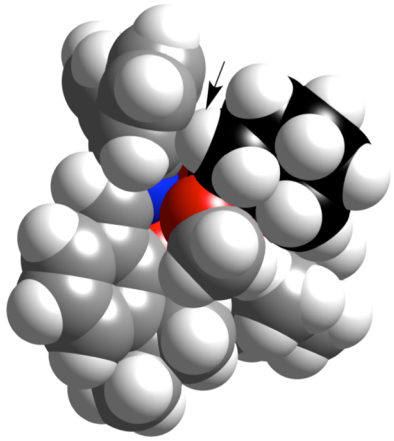

Figure 9. Optimized M06-L structure for the TS for ROP of CL by compound **G** drawn as a space-filling model (using CPK van der Waals radii). The CL ring carbons are highlighted in black, with the key destabilizing interaction of a CL hydrogen with the ligand aromatic ring indicated by an arrow.

is apparent that one phenyl ring associated with the backbone bridge of the ligand is thrust into the space that the reacting alkoxide and CL moieties (not present in the framework distortion calculation) occupy and that there is a steric clash between a CL hydrogen and that ring. Failure to account for such interactions is a drawback of the simple framework distortion energy metric.

Nevertheless, in addition to being of interest from a fundamental mechanistic standpoint, the relationship between framework distortion energy and apparent rate constants we have discovered suggests a strategy for *in silico* catalyst design. To the extent that all of the various TS structures are geometrically similar to one another about aluminum, one could use the "average" set of TS bond angles described above for framework distortion calculations with arbitrary ligands without the added expense of actually finding a true TS structure. That is, one could compute a resting catalyst structure for a given ligand of choice, remove the alkoxide, and then compute the energy to distort the resulting structure to a pseudo-TS structure having the fixed "average" angles about Al, but all other degrees of freedom relaxed. While one might expect correlation with the proper free energies of activation to degrade with such limited relaxation, certainly ligands predicted to lead to very small framework distortion energies by this rapid computational screening technique would be higher priorities for initial experimental discovery efforts.

CONCLUSIONS

With the aim of understanding how linker length influences the ROP of lactones by single-site (salen)AlOR catalysts, we evaluated the kinetics for ROP of CL by **2** under conditions that enabled determination of K_{eq} and k_2 (eq 1) as a function of temperature and electron-withdrawing capabilities of remote substituents. Comparison of these and derived thermodynamic parameters for ROP by **2** to those previously reported for **1**, which features a shorter linker, revealed similar dependences of K_{eq} and k_2 on the substituents (little variation of K_{eq}, similar Hammett parameters for k_2 of +1.4(1) and +1.2(1) for **1** and **2**, respectively). However, an overall significant increase in rate (k_2 values) was observed for **2** relative to **1**. Theoretical calculations accurately replicated the different reactant geometries for analogues **1′** and **2′** but showed that the ROP transition state structures were very similar, thus raising the possibility that the differing activation energies for the two catalysts arise from differences in the energies required to distort the ligand framework to adopt the requisite TS geometries. Support for this notion was obtained by approximating the energy cost of distorting the ligand framework from its reactant geometry to that of the TS for **1′** and **2′** through single-point calculations. Extension of this method to a previously reported series of catalysts with varying ligand linkers yielded a good correlation between the distortion energy and the rate of ROP of LA. We suggest that this relatively simple method for evaluating the ligand framework distortion energy may have even broader utility for predicting the reactivity of metal alkoxide catalysts for cyclic ester ROP reactions and is therefore a potentially useful tool for future catalyst design.

EXPERIMENTAL SECTION

Materials and Methods. General Considerations. Experiments were conducted under an inert atmosphere using a drybox or Schlenk line unless otherwise indicated. Reagents were purchased commercially and used without further purification unless otherwise stated. CL was purified by distillation from CaH_2 and stored under N_2. Deuterated solvents were dried over CaH_2 or sodium metal, distilled under vacuum, and stored under N_2. Protiated solvents were degassed and passed through a solvent purification system (Glass Contour, Laguna, CA) prior to use. ^{1}H and ^{13}C NMR spectra were recorded on a Bruker Avance III HD 500 MHz spectrometer equipped with a Prodigy TCI cryoprobe. Chemical shifts for ^{1}H and ^{13}C NMR spectra were referenced to residual protium in the deuterated solvent and deuterated solvent itself, respectively. ^{1}H NMR spectra for the kinetic runs were recorded on a Bruker Avance III 500 MHz spectrometer equipped with either a BBFO SmartProbe or a TBO triple-resonance PFG probe. ^{27}Al NMR spectra were recorded on a Bruker Avance III 500 MHz spectrometer equipped with a TBO triple-resonance PFG probe. Chemical shifts for ^{27}Al NMR spectra were externally referenced to aluminum tris(acetylacetonate) in toluene-d_8. 2-Hydroxy-3-(*tert*-butyl)-5-methoxybenzaldehyde,[12] 2-hydroxy-3-(*tert*-butyl)-5-bromobenzaldehyde,[13] and 2-hydroxy-3-(*tert*-butyl)-5-nitrobenzaldehyde[14] were synthesized according to literature procedures. Elemental analyses were performed by Robertson Microlit Laboratory (Ledgewood, NJ).

Syntheses of Proligands H_2L^{OMe}, H_2L^{Br}, and H_2L^{NO2}. In an oven-dried round-bottom flask equipped with a reflux condenser, the salicylaldehyde (H_2L^{OMe}, 1.583 g, 7.6 mmol; H_2L^{Br}, 1.311 g, 5.1 mmol; H_2L^{NO2}, 1.473 g, 6.6 mmol) was dissolved in absolute ethanol to give an approximate 0.64 M concentration. To this mixture 2,2-dimethyl-1,3-propanediamine (H_2L^{OMe}, 0.388 g, 3.8 mmol; H_2L^{Br}, 0.266 g, 2.6 mmol; H_2L^{NO2}, 0.337 g, 3.3 mmol) was added with stirring, and the solution was heated to reflux for 2 h. The reaction mixture was cooled to ambient temperature and left to sit overnight at −30 °C, yielding a

DOI: 10.1021/acscatal.5b02607
ACS Catal. 2016, 6, 1215−1224

precipitate. The crude precipitate was isolated by vacuum filtration and washed with hexanes (40 mL) before recrystallization from minimal dichloromethane (approximately 5 mL) layered with an equal volume of hexanes at −30 °C overnight. The purified product was isolated by vacuum filtration, dried overnight in a vacuum oven at ambient temperature, and stored under N_2 in a drybox as a bright yellow, crystalline solid. Yields: H_2L^{OMe}, 0.197 g, (70%); H_2L^{Br}, 1.355 g (91%); H_2L^{NO2}, 1.246 g, (73%).

H_2L^{OMe}: ^{1}H NMR (500 MHz, toluene-d_8) δ 13.82 (s, 2H, O*H*), 7.78 (s, 2H, C*H*═N), 7.16 (d, J = 3.0 Hz, 2H, Ar*H*), 6.41 (d, J = 3.0 Hz, 2H, Ar*H*), 3.49 (s, 6H, ArOCH_3), 3.10 (s, 4H, NCH_2C-(CH_3)$_2$CH_2N), 1.57 (s, 18H, Ar-*t-Bu*), 0.89 (s, 6H, NCH_2C-(CH_3)$_2$CH_2N); ^{13}C NMR (125 MHz, toluene-d_8) δ 166.76, 155.52, 152.06, 139.20, 118.66, 118.56, 111.97, 68.30, 55.25, 35.98, 35.34, 29.57, 24.45. Anal. Calcd for $C_{29}H_{42}N_2O_4$: C, 72.17; H, 8.77; N, 5.80. Found: C, 72.09; H, 8.69; N, 5.73.

H_2L^{Br}: ^{1}H NMR (500 MHz, toluene-d_8) δ 14.21 (s, 2H, O*H*), 7.51 (d, J = 2.3 Hz, 2H, Ar*H*), 7.47 (s, 2H, C*H*═N), 6.94 (d, J = 2.3 Hz, 2H, Ar*H*), 2.98 (s, 4H, NCH_2C(CH_3)$_2$CH_2N), 1.43 (s, 18H, Ar-*t-Bu*), 0.79 (s, 6H, NCH_2C(CH_3)$_2$CH_2N); ^{13}C NMR (125 MHz, toluene-d_8) δ 165.80, 160.08, 140.47, 132.78, 132.23, 120.43, 110.44, 68.06, 35.90, 35.30, 29.25, 24.18. Anal. Calcd for $C_{27}H_{36}Br_2N_2O_2$: C, 55.87; H, 6.25; N, 4.83. Found: C, 55.90; H, 6.28; N, 4.83.

H_2L^{NO2}: ^{1}H NMR (500 MHz, toluene-d_8) δ 15.27 (s, 2H, O*H*), 8.29 (d, J = 3.0 Hz, 2H, Ar*H*), 7.79 (d, J = 3.0 Hz, 2H, Ar*H*), 7.38 (s, 2H, C*H*═N), 2.93 (s, 4H, NCH_2C(CH_3)$_2$CH_2N), 1.42 (s, 18H, Ar-*t-Bu*), 0.74 (s, 6H, NCH_2C(CH_3)$_2$CH_2N); ^{13}C NMR (125 MHz, toluene-d_8) δ 167.16, 166.14, 139.61, 139.53, 126.40, 125.21, 117.34, 66.98, 35.82, 35.36, 28.98, 23.88. Anal. Calcd for $C_{27}H_{36}N_4O_6$: C, 63.26; H, 7.08; N, 10.93. Found: C, 62.64; H, 6.91; N, 10.79.

Syntheses of Complexes 2. In a glovebox, in an oven-dried 25 mL screw cap bomb flask equipped with a stirbar, equimolar amounts of proligand (H_2L^{OMe}, 0.241 g, 0.5 mmol; H_2L^{Br}, 0.290 g, 0.5 mmol; H_2L^{NO2}, 0.256 g, 0.5 mmol) and aluminum tris(isopropoxide) (0.010 g, 0.5 mmol) were dissolved in toluene (3 mL). The sealed vessel was removed from the glovebox and heated to 90 °C, and the mixture was stirred at this temperature for 3 days. After being cooled to ambient temperature, the reaction mixture was returned to the glovebox and solvent was removed in vacuo. The crude solid was purified by trituration with pentane (5 mL) and then recrystallized from minimal toluene (approximately 4 mL) layered with an equal volume of pentane at −40 °C overnight. The purified product was isolated by vacuum filtration, dried overnight on a vacuum line, and stored under N_2 in the glovebox at −40 °C as a bright yellow (R = OMe), yellow (R = Br), or light brown (R = NO_2) solid. Yields: R = OMe, 0.230 g; (81%); R = Br, 0.184 g (72%); R = NO_2, 0.263 g, (90%).

2 (R = OMe): ^{1}H NMR (500 MHz, toluene-d_8) δ 7.48 (s, 2H, C*H*═N), 7.36 (d, J = 3.2 Hz, 2H, Ar*H*), 6.30 (d, J = 3.2 Hz, 2H, Ar*H*), 4.13 (septet, J = 5.2 Hz, 1H, OC*H*(CH_3)$_2$), 3.50 (s, 6H, ArOCH_3), 3.38 (d, J = 12.1 Hz, 2H, NCH′*H*C(CH_3)$_2$CH′*H*N), 2.73 (d, J = 12.1 Hz, 2H, NC*H*′HC(CH_3)$_2$C*H*′HN), 1.72 (s, 18H, Ar-*t-Bu*), 1.17 (d, 5.2 Hz, 6H, OCH(CH_3)$_2$), 0.80 (s, 3H, NCH_2C-(CH_3)′(CH_3)CH_2N), 0.54 (s, 3H, NCH_2C(CH_3)′(CH_3)CH_2N); ^{13}C NMR (125 MHz, toluene-d_8) δ 169.35, 161.44, 150.33, 143.24, 123.17, 118.37, 111.30, 68.09, 62.95, 55.25, 35.95, 35.65, 30.17, 29.98, 25.62, 25.21; ^{27}Al NMR (130 MHz, toluene-d_8) δ 35.33. Anal. Calcd for $C_{32}H_{47}AlN_2O_5$: C, 67.82; H, 8.36; N, 4.94. Found: C, 67.81; H, 8.32; N, 4.89.

2 (R = Br): ^{1}H NMR (500 MHz, toluene-d_8) δ 7.63 (d, J = 2.6 Hz, 2H, Ar*H*), 7.17 (s, 2H, C*H*═N), 6.89 (d, J = 2.6 Hz, 2H, Ar*H*), 3.97 (septet, J = 5.9 Hz, 1H, OC*H*(CH_3)$_2$), 3.25 (d, J = 12.1 Hz, 2H, NCH′*H*C(CH_3)$_2$CH′*H*N), 2.59 (d, J = 12.1 Hz, 2H, NC*H*′HC-(CH_3)$_2$C*H*′HN), 1.56 (s, 18H, Ar-*t-Bu*), 1.08 (d, 6.0 Hz, 6H, OCH(CH_3)$_2$), 0.72 (s, 3H, NCH_2C(CH_3)′(CH_3)CH_2N), 0.47 (s, 3H, NCH_2C(CH_3)′(CH_3)CH_2N); ^{13}C NMR (125 MHz, toluene-d_8) δ 168.85, 164.63, 144.34, 135.59, 133.47, 120.92, 108.07, 67.89, 63.10, 35.91, 35.50, 29.66, 28.20, 25.55, 25.07; ^{27}Al NMR (130 MHz, toluene-d_8) δ 33.63. Anal. Calcd for $C_{30}H_{41}AlBr_2N_2O_3$: C, 54.23; H, 6.22; N, 4.22. Found: C, 54.29; H, 6.27; N, 4.22.

2 (R = NO_2): ^{1}H NMR (500 MHz, toluene-d_8) δ 8.43 (d, J = 3.0 Hz, 2H, Ar*H*), 7.81 (d, J = 3.0 Hz, 2H, Ar*H*), 7.14 (s, 2H, C*H*═N), 3.85 (septet, J = 6.0 Hz, 1H, OC*H*(CH_3)$_2$), 3.21 (d, J = 12.1 Hz, 2H, NCH′*H*C(CH_3)$_2$CH′*H*N), 2.59 (d, J = 12.1 Hz, 2H, NC*H*′HC-(CH_3)$_2$C*H*′HN), 1.53 (s, 18H, Ar-*t-Bu*), 1.04 (d, 6.0 Hz, 6H, OCH(CH_3)$_2$), 0.71 (s, 3H, NCH_2C(CH_3)′(CH_3)CH_2N), 0.50 (s, 3H, NCH_2C(CH_3)′(CH_3)CH_2N); ^{13}C NMR (125 MHz, toluene-d_8) δ 169.70, 169.48, 142.80, 138.23, 129.18, 127.39, 118.22, 67.80, 63.28, 35.91, 35.42, 29.41, 27.98, 25.56, 25.01; ^{27}Al NMR (130 MHz, toluene-d_8) δ 33.40. Anal. Calcd for $C_{30}H_{41}AlN_4O_7$: C, 60.39; H, 6.93; N, 9.39. Found: C, 60.15; H, 6.55; N, 8.71.

Kinetics Measurements and Analysis. A procedure for a typical kinetic run is as follows. In a nitrogen-filled glovebox, an NMR tube dried in a vacuum oven at ambient temperature was charged with 500 μL of a stock solution of catalyst in toluene-d_8 (0.0098 M) and 10 μL of the internal standard 1,4-bis(trimethylsilyl)benzene in toluene-d_8 (0.28 M). The NMR tube was capped with a septum and wrapped with black electric tape. A gastight syringe was loaded with 190 μL of a stock solution of ε-caprolactone (CL) in toluene-d_8 (7.4 M) and capped with a septum to prevent air contamination during the experiment setup. The target concentrations for the NMR reaction were 0.007 M catalyst, 0.004 M internal standard, and 2.0 M CL. The NMR tube and loaded syringe were taken out of the glovebox and brought to the spectrometer. A pure methanol standard was used to calibrate the temperature of the spectrometer (500 MHz Bruker Avance III). In order to accurately determine catalyst concentration, a relaxation relay of 10 s was used to ensure complete relaxation for quantification integrations. A ^{1}H NMR spectrum of the catalyst and internal standard was measured, and then the NMR tube was ejected from the spectrometer and CL was injected through the septum. The NMR tube was aggressively shaken and inverted before being reinserted into the spectrometer. The time between the CL injection and the start of ^{1}H NMR data acquisition was recorded in minutes. An array of spectra was taken every 48 s (four scans) for most kinetic runs except for the runs with R = NO_2 (288, 293 K) and R = Br (273 K), where a spectrum was taken every 24 s (two scans) and 96 s (eight scans), respectively. The acquisition parameters were as follows: relaxation delay 10 s, 30° pulse width 3.9, gain of 10 or 16 depending on the NMR probe used, and acquisition time 2 s. Samples were spun, and autoshim was employed to allow for shimming during kinetic runs. The arrayed experiment was allowed to proceed until the disappearance of the CL peaks, indicating complete polymerization. For R = NO_2 (273 K), the kinetic runs were halted prior to the complete disappearance of CL peaks due to the loss of shims by the spectrometer. For each catalyst, triplicate reactions were performed at four different temperatures. The obtained arrayed NMR data were phased and baseline corrected before being integrated, using Mestrenova (http://mestrelab.com/). Using the peak integrations, absolute concentrations of all species as a function of time were calculated relative to the concentration of internal standard. The reaction time was calculated in seconds from the known duration of each spectrum and the time between the CL injection and the start of the ^{1}H NMR data acquisition. The concentration vs time data were entered into the program COPASI and fit to eq S1 in the Supporting Information to obtain K_M and V_{max} values. The reaction rates were calculated using eq S1 and plotted as a function of [CL]; full details of the fits and results are provided as Supporting Information. All linear and nonlinear curve fits were performed using Origin 9.1 SR2 software (OriginLab, Northampton, MA).

Binding Study with γ-Butyrolactone. In a nitrogen-filled glovebox, six NMR tubes dried in a vacuum oven at ambient temperature were each charged with 500 μL of a stock solution of catalyst **2** (R = OMe, Br, NO_2) in toluene-d_8 (0.0074−0.0078 M). Different amounts (10−190 μL) of a 7.38 M stock solution of γ-butyrolactone (BL) were added to each tube. Toluene-d_8 was added to some of the tubes to achieve an overall volume of 690 μL. The NMR tubes were capped and shaken. The final concentrations for BL were 0.11, 0.25, 0.50, 0.75, 1.0, 1.5, and 2.0 M, while the catalyst concentration ranged from 0.005 to 0.007 M. The reactions were monitored at 293 K by ^{1}H NMR spectroscopy (500 MHz Bruker

DOI: 10.1021/acscatal.5b02607
ACS Catal. 2016, 6, 1215−1224

Avance III) using the same parameters as the kinetic runs. This experiment was run in triplicate for each catalyst, and the spectra were processed using Mestrenova and analyzed by NMR peak analysis using Origin 9.1 SR2 software.

Density Functional Calculations. Molecular structures were optimized at the M06-L level[15] of density functional theory employing the 6-31+G(d,p) basis set.[16] The nature of all stationary points was confirmed by computation of analytic vibrational frequencies, which were also employed to compute vibrational contributions to the molecular partition function, replacing all vibrations below 50 cm^{-1} with values of 50 cm^{-1} in order to correct for the well-known deficiency of the quantum mechanical harmonic oscillator approximation when applied to very low frequency motions.[17] Improved free energies were computed by summing thermal contributions from this lower level of theory with single-point electronic energies computed at the M06-2X level[18] of density functional theory employing the 6-311+G(d,p) basis set.[16] Solvation effects for toluene as solvent were included during single-point energy calculations employing the SMD solvation model.[19]

There are a very large number of conformational and configurational possibilities associated with the binding of the catalyst with caprolactone. In this work, we consider a limited number of structures, primarily to compare with prior work involving a different, but analogous, catalyst. A more exhaustive survey of the various possible complexes and reaction paths undertaken for an analogue of the catalyst in this work from which alkyl groups substituting the ligand were removed suggests that the specific structures reported in this study are indeed relevant as low-energy stationary points, and results from that work on the reduced catalyst are summarized in the Supporting Information.

Calculations were carried out with the Gaussian 09 suite of electronic structure programs.[20] CM5 charges were computed using the auxiliary CM5PAC program.[21]

■ ASSOCIATED CONTENT

Supporting Information

The Supporting Information is available free of charge on the ACS Publications website at DOI: 10.1021/acscatal.5b02607.

X-ray data (CIF)

Spectroscopic and kinetics data and fits and computational details (PDF)

■ AUTHOR INFORMATION

Corresponding Authors

*E-mail for C.J.C.: cramer@umn.edu.

*E-mail for M.A.H.: hillmyer@umn.edu.

*E-mail for W.B.T.: wtolman@umn.edu.

Notes

The authors declare no competing financial interest.

■ ACKNOWLEDGMENTS

Funding for this project was provided by the Center for Sustainable Polymers, a National Science Foundation supported Center for Chemical Innovation (CHE-1413862). The X-ray diffraction experiments were performed using a crystal diffractometer acquired through NSF-MRI Award CHE-1229400. The NMR experiments were performed on Bruker Avance III 500 MHz spectrometers acquired through NIH Award S10OD011952. We thank Dr. Letitia Yao for her help with NMR kinetics experiments.

■ REFERENCES

(1) *Handbook of Ring-Opening Polymerization*; Dubois, P., Coulembier, O., Raquez, J.-M., Eds.; Wiley: Weinheim, Germany, 2009.

(2) Selected recent reviews: (a) Kiesewetter, M. K.; Shin, E. J.; Hedrick, J. L.; Waymouth, R. M. *Macromolecules* **2010**, *43*, 2093−2107. (b) Thomas, C. M. *Chem. Soc. Rev.* **2010**, *39*, 165−173. (c) Dijkstra, P. J.; Du, H.; Feijen, J. *Polym. Chem.* **2011**, *2*, 520−527. (d) Buchard, A.; Bakewell, C.; Weiner, J.; Williams, C. In *Topics in Organometallic Chemistry: Organometallics and Renewables*; Meier, M. A. R., Weckhuysen, B. M., Bruijnincx, P. C. A., Eds.; Springer: Berlin, Heidelberg, 2012; Vol. *39*, pp 175−224. (e) Dagorne, S.; Normand, M.; Kirillov, E.; Carpentier, J.-F. *Coord. Chem. Rev.* **2013**, *257*, 1869−1886. (f) Sauer, A.; Kapelski, A.; Fliedel, C.; Dagorne, S.; Kol, M.; Okuda, J. *Dalton Trans.* **2013**, *42*, 9007−17. (g) Hillmyer, M. A.; Tolman, W. B. *Acc. Chem. Res.* **2014**, *47*, 2390−2396. (h) Guillaume, S. M.; Kirillov, E.; Sarazin, Y.; Carpentier, J.-F. *Chem. - Eur. J.* **2015**, *21*, 7988−8003.

(3) (a) Borner, J.; Florke, U.; Gloge, T.; Bannenberg, T.; Tamm, M.; Jones, M. D.; Doring, A.; Kuckling, D.; Herres-Pawlis, S. *J. Mol. Catal. A: Chem.* **2010**, *316*, 139−145. (b) Altenbuchner, P. T.; Kronast, A.; Kissling, S.; Vagin, S. I.; Herdtweck, E.; Poethig, A.; Deglmann, P.; Loos, R.; Rieger, B. *Chem. - Eur. J.* **2015**, *21*, 13609−13617. (c) Chang, M. C.; Lu, W. Y.; Chang, H. Y.; Lai, Y. C.; Chiang, M. Y.; Chen, H. Y.; Chen, H. Y. *Inorg. Chem.* **2015**, *54*, 11292−11298. (d) Horeglad, P.; Cybularczyk, M.; Trzaskowski, B.; Zukowska, G. Z.; Dranka, M.; Zachara, J. *Organometallics* **2015**, *34*, 3480−3496. (e) Roymuhury, S. K.; Chakraborty, D.; Ramkumar, V. *Eur. Polym. J.* **2015**, *70*, 203−214. (f) Tabthong, S.; Nanok, T.; Sumrit, P.; Kongsaeree, P.; Prabpai, S.; Chuawong, P.; Hormnirun, P. *Macromolecules* **2015**, *48*, 6846−6861.

(4) Hormnirun, P.; Marshall, E. L.; Gibson, V. C.; Pugh, R. I.; White, A. J. P. *Proc. Natl. Acad. Sci. U. S. A.* **2006**, *103*, 15343−15348.

(5) Ding, K.; Miranda, M. O.; Moscato-Goodpaster, B.; Ajellal, N.; Breyfogle, L. E.; Hermes, E. D.; Schaller, C. P.; Roe, S. E.; Cramer, C. J.; Hillmyer, M. A.; Tolman, W. B. *Macromolecules* **2012**, *45*, 5387−5396.

(6) Miranda, M. O.; DePorre, Y.; Vazquez-Lima, H.; Johnson, M. A.; Marell, D. J.; Cramer, C. J.; Tolman, W. B. *Inorg. Chem.* **2013**, *52*, 13692−13701.

(7) Addison, A. W.; Rao, T. N.; Reedijk, J.; van Rijn, J.; Verschoor, G. C. *J. Chem. Soc., Dalton Trans.* **1984**, 1349−1356.

(8) (a) Nomura, N.; Ishii, R.; Yamamoto, Y.; Kondo, T. *Chem. - Eur. J.* **2007**, *13*, 4433−4451. (b) Du, H.; Pang, X.; Yu, H.; Zhuang, X.; Chen, X.; Cui, D.; Wang, X.; Jing, X. *Macromolecules* **2007**, *40*, 1904−1913. (c) Chen, H.-L.; Dutta, S.; Huang, P.-Y.; Lin, C.-C. *Organometallics* **2012**, *31*, 2016−2025. (d) Agatemor, C.; Arnold, A. E.; Cross, E. D.; Decken, A.; Shaver, M. P. *J. Organomet. Chem.* **2013**, *745−746*, 335−340.

(9) Blackmond, D. *Angew. Chem., Int. Ed.* **2005**, *44*, 4302−4320.

(10) (a) Duda, A.; Biela, T.; Libiszowski, J.; Penczek, S.; Dubois, P.; Mecerreyes, D.; Jérôme, R. *Polym. Degrad. Stab.* **1998**, *59*, 215−222. (b) Saiyasombat, W.; Molloy, R.; Nicholson, T. M.; Johnson, A. F.; Ward, I. M.; Poshyachinda, S. *Polymer* **1998**, *39*, 5581−5585. (c) Houk, K. N.; Jabbari, A.; Hall, H. K., Jr.; Alemán, C. *J. Org. Chem.* **2008**, *73*, 2674−2678. (d) Alemán, C.; Betran, O.; Casanovas, J.; Houk, K. N.; Hall, H. K., Jr. *J. Org. Chem.* **2009**, *74*, 6237−6244.

(11) (a) We did examine whether the two different ligands had differing electronic influences on the natures of the precatalyst or TS structures. However, CM5 partial atomic charges (see ref 10b) computed for corresponding species showed essentially no variation as a function of ligand, leading us to focus more closely on steric/geometric influences.. (b) Marenich, A. V.; Jerome, S. V.; Cramer, C. J.; Truhlar, D. G. *J. Chem. Theory Comput.* **2012**, *8*, 527−541.

(12) Kurahashi, T.; Fujii, H. *J. Am. Chem. Soc.* **2011**, *133*, 8307−8316.

(13) Cavazzini, M.; Manfredi, A.; Montanari, F.; Quici, S.; Pozzi, G. *Eur. J. Org. Chem.* **2001**, *2001*, 4639−4649.

(14) Braun, M.; Fleischer, R.; Mai, B.; Schneider, M.-A.; Lachenicht, S. *Adv. Synth. Catal.* **2004**, *346*, 474−482.

(15) Zhao, Y.; Truhlar, D. G. *J. Chem. Phys.* **2006**, *125*, 194101.

(16) Hehre, W. J.; Radom, L.; Schleyer, P. v. R.; Pople, J. A. *Ab Initio Molecular Orbital Theory*; Wiley: New York, 1986; pp 65−88.

DOI: 10.1021/acscatal.5b02607
ACS Catal. 2016, 6, 1215−1224

(17) (a) Cramer, C. J. *Essentials of Computational Chemistry: Theories and Models*, 2nd ed.; Wiley: Chichester, U.K., 2004; pp 375−377. (b) Ribeiro, R. F.; Marenich, A. V.; Cramer, C. J.; Truhlar, D. G. *J. Phys. Chem. B* **2011**, *115*, 14556−14562.
(18) Zhao, Y.; Truhlar, D. G. *Theor. Chem. Acc.* **2008**, *120*, 215−241.
(19) Marenich, A. V.; Cramer, C. J.; Truhlar, D. G. *J. Phys. Chem. B* **2009**, *113*, 6378−6396.
(20) Frisch, M. J.; Trucks, G. W.; Schlegel, H. B.; Scuseria, G. E.; Robb, M. A.; Cheeseman, J. R.; Scalmani, G.; Barone, V.; Mennucci, B.; Petersson, G. A.; Nakatsuji, H.; Caricato, M.; Li, X.; Hratchian, H. P.; Izmaylov, A. F.; Bloino, J.; Zheng, G.; Sonnenberg, J. L.; Hada, M.; Ehara, M.; Toyota, K.; Fukuda, R.; Hasegawa, J.; Ishida, M.; Nakajima, T.; Honda, Y.; Kitao, O.; Nakai, H.; Vreven, T.; Montgomery, J. A.; Peralta, J. E.; Ogliaro, F.; Bearpark, M.; Heyd, J. J.; Brothers, E.; Kudin, K. N.; Staroverov, V. N.; Kobayashi, R.; Normand, J.; Raghavachari, K.; Rendell, A.; Burant, J. C.; Iyengar, S. S.; Tomasi, J.; Cossi, M.; Rega, N.; Millam, J. M.; Klene, M.; Knox, J. E.; Cross, J. B.; Bakken, V.; Adamo, C.; Jaramillo, J.; Gomperts, R.; Stratmann, R. E.; Yazyev, O.; Austin, A. J.; Cammi, R.; Pomelli, C.; Ochterski, J. W.; Martin, R. L.; Morokuma, K.; Zakrzewski, V. G.; Voth, G. A.; Salvador, P.; Dannenberg, J. J.; Dapprich, S.; Daniels, A. D.; Farkas, Ö.; Foresman, J. B.; Ortiz, J. V.; Cioslowski, J.; Fox, D. J. *Gaussian 09, Revision C.01*; Gaussian, Inc., Wallingford, CT, 2010.
(21) Marenich, A. V.; Cramer, C. J.; Truhlar, D. G. *CM5PAC*; University of Minnesota, Minneapolis, MN, 2011.

DOI: 10.1021/acscatal.5b02607
ACS Catal. 2016, 6, 1215−1224